JOURNAL OF CATALYSIS 136, 96–109 (1992)

Study of Carbonaceous Deposits on Fischer–Tropsch Oxide-Supported Iron Catalysts

J. GALUSZKA, T. SANO,* AND J. A. SAWICKI†

*Energy Research Laboratories, CANMET, Energy, Mines and Resources Canada, Ottawa, Ontario, Canada K1A 0G1; *NSERC Fellow from National Chemical Laboratory for Industry, Tsukuba, Ibaraki 305, Japan; and †AECL Research, Chalk River Laboratories, Chalk River, Ontario, Canada K0J 1J0*

Received August 14, 1990; revised February 18, 1992

Fischer–Tropsch synthesis was performed at semi-industrial conditions (300°C, 1515 kPa, $H_2/CO = 1$) on various oxide (SiO_2, Al_2O_3, TiO_2, ZrO_2)-supported iron catalysts. The carbonaceous materials deposited on the catalysts after 260 h on stream were characterized by FTIR spectroscopy and thermogravimetry during temperature-programmed oxidation, and by ^{57}Fe Mössbauer spectroscopy. The characteristics of the carbonaceous deposits were strongly affected by the nature of the catalyst supports. At least five different forms of carbonaceous materials have been identified: aliphatic, aromatic, oxygenated, carbidic, and amorphous. Iron carbides have been found in all used catalysts. Mössbauer spectra of all used catalysts after heating in air at 400°C showed reoxidation of all carbides to α-Fe_2O_3. A tentative correlation of the carbonaceous deposit characteristics with the nature of the catalyst supports is offered.

INTRODUCTION

When a supported metal catalyst is exposed to a reaction mixture containing carbon monoxide or hydrocarbons at high temperature, various forms of carbonaceous materials are deposited on the catalyst surface. Some forms of such deposits cause catalyst deactivation, whereas others assist and are indeed necessary for the chemical reaction to proceed. Deactivation of catalysts by carbonaceous deposits is a problem of serious magnitude for the petroleum industry in the conversion of coal and heavy feedstocks to clean fuels, in steam reforming, in Fischer–Tropsch synthesis, and in many other important catalytic processes, as is evidenced by the fairly extensive published literature [e.g., (*1–15*)].

In spite of considerable effort many questions remain to be answered concerning the chemical, physical, and morphological properties of various carbonaceous materials. Various factors relevant to the nature of the catalyst supports, which may play a significant role in shaping the characteristics of carbonaceous materials, are not straightforwardly understood. Also, a specific knowledge of carbonaceous deposits related to catalysts performing under industrial conditions appears not to be well represented in the open literature. For example, data for the supported iron catalysts tested during prolonged Fischer–Tropsch synthesis are scarce.

The objective of this study was to determine the effect of silica, alumina, titania, and zirconia supports on the characteristics of carbonaceous materials. The characterization of these materials, deposited during 260 h on stream on supported iron Fischer–Tropsch catalysts tested under semi-industrial conditions, was carried out by FTIR spectroscopy and thermogravimetry during temperature-programmed oxidation. In addition, ^{57}Fe Mössbauer spectroscopy was employed to obtain the data related to the chemical state of iron on the catalyst.

0021-9517/92 $5.00

TABLE 1

Characteristics of Fresh Catalyst Powders

Catalyst	Fe (wt%)	BET surface area (m^2/g-cat)
Fe/SiO_2	4.99	273
Fe/Al_2O_3	5.16	223
Fe/TiO_2	5.15	46
Fe/ZrO_2	5.06	3.2

EXPERIMENTAL

Materials

The oxide (Al_2O_3, SiO_2, TiO_2, ZrO_2)-supported 5 wt% iron catalysts were prepared by the conventional impregnation method. The following reagents were used; $Fe(NO_3)_3$ $9H_2O$ (B.D.H. Chemicals Canada, guaranteed reagent), SiO_2 (Davison Specialty Chemical Co., Grade 57), γ-Al_2O_3 (Kaiser Chemicals, Versal GH), TiO_2 (Degussa Canada Ltd., P-25), and ZrO_2 (Alfa Division, Ventron Co.). The required amount of a support was dried at 150°C for 24 h. A given amount of aqueous solution of $Fe(NO_3)_3$ was slowly poured over the dry supports with gentle and even mixing. Then, the catalyst pastes were air-dried at 90°C for 24 h in an oven. After drying, the catalysts were calcined at 450°C for 24 h and sized to give 70–100 mesh fraction. The catalyst powders were mixed with stearic acid (1–5 wt%), pelletized to 3 × 4 mm pellets, and calcined at 450°C for 20 h. As the silica-supported iron catalyst did not pelletize well, the catalyst after calcination was milled and a 6–8 mesh sample was collected. These materials are referred to as "fresh catalysts." Before pelletizing, all catalyst powders were analyzed for metal content by atomic absorption and BET surface area by nitrogen adsorption. The results are given in Table 1.

Apparatus and Procedure

Catalyst performance in the Fischer–Tropsch synthesis was tested in a high-pressure, fully automated computer-controlled, fixed-bed down-flow reactor system. Conversion of the synthesis gas was carried out at 300°C, 1515 kPa pressure, and a H_2/CO ratio of 1. Steady state was reached after 50 to 100 h on stream and was maintained throughout the duration of all the runs. CO conversions after steady state was reached were 75, 40, 35, and 25% for ZrO_2, SiO_2, Al_2O_3, and TiO_2-supported catalysts, respectively. The effective H_2/CO ratio remained between 0.9 and 1.2 as measured at the reactor exit. The computer-controlled six zone furnace with heating and cooling action gave temperature profiles of the catalyst beds within ±5°C. Only the Fe/SiO_2 and Fe/ZrO_2 catalysts developed occasional hot points at the top edge of the bed as temperature raised to 330 and 350°C, respectively. Further experimental details and the reactor system used are described elsewhere (*16*).

After 260 h on stream the catalysts were flushed with argon for 30 min at 300°C then cooled to room temperature in flowing argon. Used catalysts were removed from the reactor and subjected to further tests. Each catalyst bed was 300 mm long in the 25-mm inside diameter reactor. Each bed was divided into four 75-mm axial sections upon removal. Samples taken from each section were kept separate and subjected to all tests described below. No substantial differences were observed between representative samples taken from different sections of the catalyst bed. Only the Fe/SiO_2 and Fe/ZrO_2 catalysts removed from the top section of the catalyst bed showed higher amounts of the carbonaceous deposits than the other sections of the bed, most likely due to the hot points described above. All the experimental data described in this report were obtained for the catalyst bed sections located 150–225 mm below the top of the catalyst bed.

The crystal structures of the fresh and used catalysts were analyzed by Cu$K\alpha$ X-ray diffraction. The amount of carbon and hydrogen was determined by high-temperature combustion analysis. A SEMCO, NANOLAB 7 scanning electron

microscope (SEM) was used to examine the fresh and used catalysts.

Thermogravimetric analyses (TGA) were performed with a Perkin–Elmer TGA-7 thermogravimetric analyzer from 35 to 700°C at a heating rate of 20°C/min in air or nitrogen streams flowing at 30 ml/min.

The temperature-programmed oxidation (TPO) of the carbonaceous materials deposited on the used catalysts was carried out with simultaneous infrared spectroscopy of the surface. The apparatus used was an all-metal closed circulation system incorporating a quadrupole mass spectrometer (Balzers QMG 112) and a high-/low-pressure and high-temperature infrared cell coupled to a FTIR spectrometer (Nicolet SX-60) (*17*). The catalysts were pressed into self-supporting disks (13 mm in diameter, 20–30 mg) for infrared spectroscopy measurements. Before TPO, the catalysts were evacuated at room temperature overnight and subsequently at 150°C for 2h. The TPO was carried out from 30 to 500°C at a heating rate of 10°C/min in 10.6 kPa of dry air. All infrared spectra were recorded in absorbance with a resolution of 4 cm^{-1}.

The ^{57}Fe Mössbauer transmission spectra of all catalysts in their calcined and used forms were obtained at room temperature. A 25-mCi γ-ray ^{57}Co source in a rhodium matrix was used. The 14.4-keV γ-rays were detected with a Kr–CO_2 proportional counter. The spectrometer was calibrated with a standard α-Fe absorber. The absorbers consisted of the powdered catalysts spread out over the sample support in uniform thickness of 100 mg/cm^2.

RESULTS AND DISCUSSION

Elemental and SEM Analysis

The results of elemental analysis of all used catalysts are summarized in Table 2. The amounts of carbonaceous deposits varied for each catalyst. Iron supported on ZrO_2 was the only catalyst that did not contain hydrogen. The C/Fe atomic ratio for this catalyst was about 0.5, which roughly agrees with the stoichiometry of iron carbides and might indicate that most of the iron was in the form of carbide. The Fe/SiO_2 and Fe/Al_2O_3 catalysts contained considerably more carbon, indicating a carbon content in excess of that required for carbide formation. These results suggest that the compositions of the carbonaceous materials deposited on a supported iron catalyst are strongly influenced by the nature of the catalyst support.

TABLE 2

Results of Elemental Analysis of Used Catalysts

Catalyst	C (wt%)	H (wt%)[a]	C/Fe
Fe/SiO_2	3.72	0.24	3.47
Fe/Al_2O_3	2.53	0.43	2.28
Fe/TiO_2	0.72	0.03	0.65
Fe/ZrO_2	0.59	0.00	0.54

[a] Not corrected for the presence of water.

No filamentous carbon was detected on any of the used catalysts by SEM (magnification 5×10^3). However, considerable surface reorganization as compared to the surface of fresh catalysts was very apparent.

Thermogravimetric Analysis

Figure 1 shows the results of TG analysis in which the carbonaceous materials accumulated on the used catalysts were oxidized in a stream of air between 35 and 700°C. There are significant differences between the catalysts. A derivative form of the TG curve obtained by TPO of the used Fe/SiO_2 catalyst exhibits two weight loss peaks at about 340 and 550°C, in addition to the water peak. The lower temperature weight loss peak has a composite nature, revealed by a shoulder at about 280°C. The shoulder at 280°C coincides with the position of the single weight loss peaks in the TG curves of Fe/Al_2O_3 and Fe/TiO_2 catalysts. The TG pattern of the Fe/ZrO_2 catalysts is obscured by the simultaneous presence of the weight gain and loss peaks. The weight gain can be explained by reoxidation of Hägg carbide to iron oxide. The amount of the weight

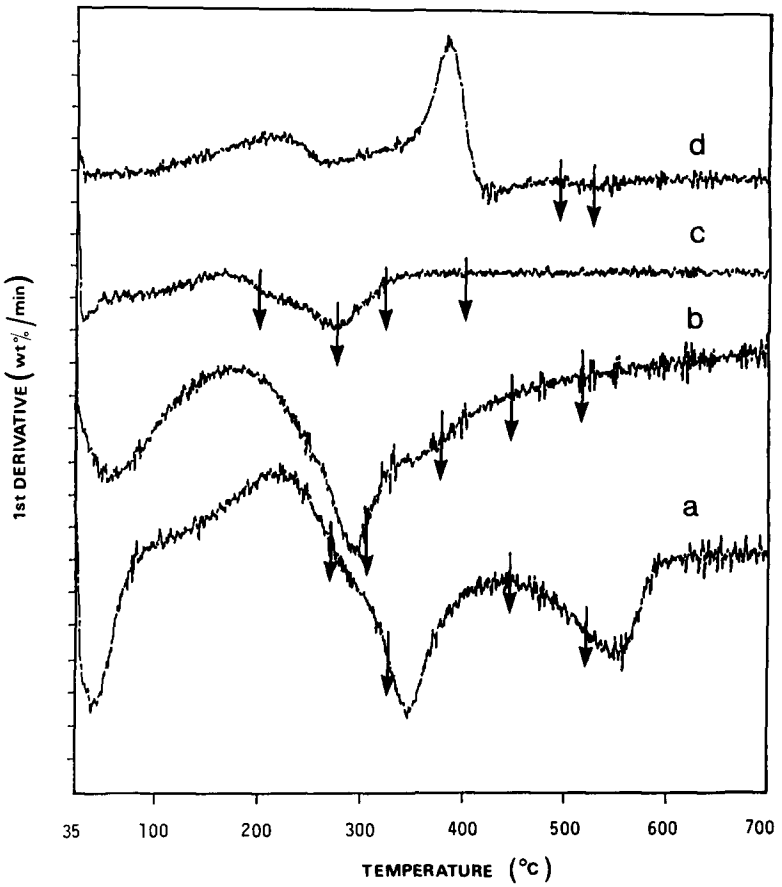

FIG. 1. TPO patterns of used catalysts: (a) Fe/SiO_2, (b) Fe/Al_2O_3, (c) Fe/TiO_2, and (d) Fe/ZrO_2. Arrows indicate the start of infrared scanning and corresponding infrared spectra are shown in Figs. 2–5.

increase agrees roughly with the stoichiometry of Fe_5C_2 to Fe_2O_3 transformation.

Infrared Spectroscopy during TPO

The conditions of the TPO experiments described in the previous paragraph were reproduced in the infrared cell. Infrared spectra were recorded at certain temperatures during TPO of the carbonaceous materials deposited on the used catalysts. The arrows on the TG curves in Fig. 1 indicate the start of infrared scanning and the corresponding infrared spectra are shown in Figs. 2–5. The peak intensities in all infrared spectra are normalized to the same catalyst mass.

Fe/SiO_2 catalyst. In the case of the used Fe/SiO_2 catalyst, several infrared bands were observed in the spectral range 3300–1200 cm^{-1} at room temperature, as shown in Fig. 2. The bands near 2926 and 2853 cm^{-1} can be assigned to asymmetric and symmetric C–H stretching vibrations in $-CH_2-$ species, respectively (*19*). The band near 2926 cm^{-1} has a shoulder near 2970 cm^{-1} which can be assigned to asymmetric C–H stretching vibration in $-CH_3$ species (*19*). The weak band near 1451 cm^{-1} can very likely be assigned to C–H deformation vibration in oligomeric $-CH_2-$ or to C–H deformation vibration in $-CH_3$ species (*20–23*). The infrared bands near 1982, 1871, and 1621 cm^{-1} arose from the SiO_2 support itself (*19*). The intensities of the bands near

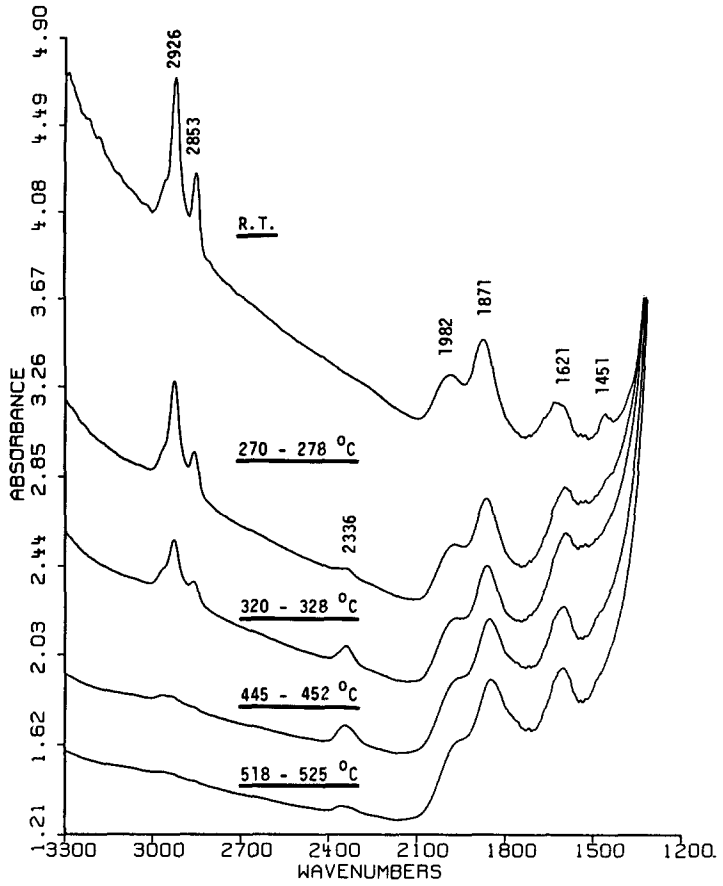

FIG. 2. Infrared spectra of carbonaceous deposits on Fe/SiO_2 used catalyst. Spectra were recorded during TPO, as indicated by arrows on curve (a) in Fig. 1. Spectra are displaced vertically for clarity.

2926, 2853, and 1451 cm^{-1} started to decrease after the temperature reached 250°C. All these bands practically disappeared from the spectra at about 450°C. The band at 2336 cm^{-1} assigned to carbon dioxide was observed only above 250°C. This temperature coincided with that of the starting point of weight loss in the TG spectrum. Obviously, carbon dioxide was a major product from oxidation of the carbonaceous materials. These results indicate that the carbonaceous materials detectable by infrared spectroscopy on the used Fe/SiO_2 catalyst are most likely saturated oligomers (*24*). These oligomers upon oxidation formed the weight loss peak at 340°C in the derivative form of the TG pattern. Since all infrared bands associated with the carbonaceous materials were removed at 450°C, the weight loss peak at 550°C must have been formed by oxidation of an infrared inactive form of the carbonaceous deposit.

Fe/Al_2O_3 catalyst. The infrared spectra of the used Fe/Al_2O_3 catalyst are shown in Fig. 3. Several bands with frequencies at 2970, 2927, 2850, 1591, 1559, 1462, and 1332 cm^{-1} were observed in the spectral range 1200–3300 cm^{-1} at room temperature. The weak bands at 2970, 2927, and 2850 cm^{-1} belong to the C–H stretching region in $-CH_3-$ and $-CH_2-$ surface species. The C–H deformation vibrations of the same species gave rise to a shoulder at about 1420 cm^{-1} and a band at 1332 cm^{-1}. The assign-

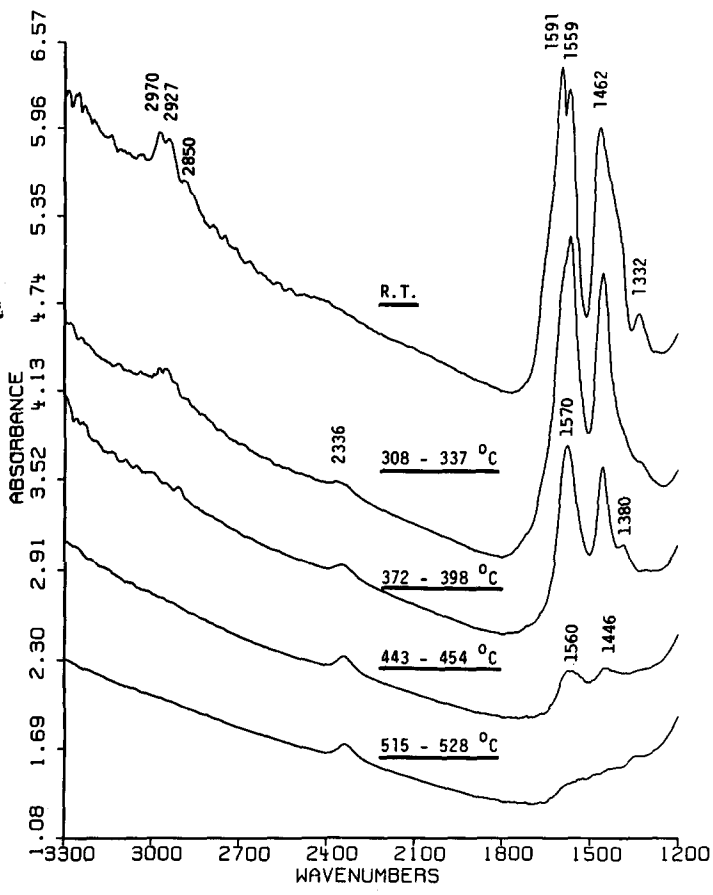

FIG. 3. Infrared spectra of carbonaceous deposits on Fe/Al_2O_3 used catalyst. Spectra were recorded during TPO, as indicated by arrows on curve (b) in Fig. 1.

ments of the strong bands at 1591, 1559, and 1462 cm^{-1} have been a controversial subject in the literature and were thoroughly discussed in the previous paper (*17*). It was concluded that these infrared bands could be assigned to C–O vibration in carboxylate type surface species (*17, 25, 26*) and aromatic ring C=C stretching vibration (*17*) in polyaromatic species. A small contribution from a surface carbonate should also be considered. The same interpretation is adopted in the present paper. As shown in Fig. 3, all infrared bands characteristic of $-CH_3$ and $-CH_2-$ surface species disappeared from the infrared spectra at 400°C. All the other bands practically vanished at 530°C. Therefore, oxidation of a saturated oligomeric form of the carbonaceous deposit constituted the weight loss peak at 280°C in the derivative form of the TG spectrum. The aromatic and carboxylate species contributed mainly to the high-temperature side tail of this peak.

Fe/TiO_2 catalyst. The infrared spectra acquired during examination of the used Fe/TiO_2 catalyst are shown in Fig. 4. The bands with frequencies at 2970, 2926, 2854, and 1305 cm^{-1} are characteristic of various modes of vibrations of the $-CH_3$ and $-CH_2-$ surface species, as described for the used Fe/Al_2O_3 catalysts. These species were practically eliminated from the catalyst surface in the course of TPO at about 330°C. The assignments of the two strongest bands

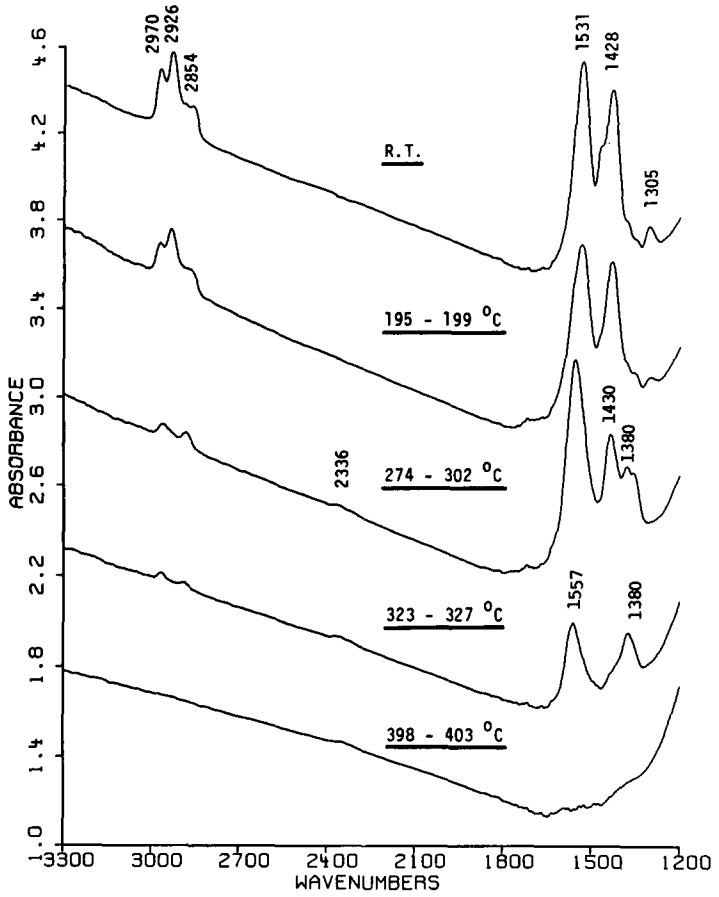

FIG. 4. Infrared spectra of carbonaceous deposits on Fe/TiO_2 used catalyst. Spectra were recorded during TPO, as indicated by arrows on curve (c) in Fig. 1.

in the spectral range below 1700 cm^{-1} near 1531 and 1428 cm^{-1} recorded at room temperature were not trivial. These bands had composite structures and they evolved during TPO into two new infrared bands with frequencies near 1557 and 1380 cm^{-1}, before vanishing from the spectra at about 400°C. This was the main difference between the species on Fe/TiO_2 and the species having similar infrared frequencies below 1700 cm^{-1} on Fe/Al_2O_3, which needed a substantially higher temperature to be removed from the catalyst surface.

In additional experiments the infrared spectra of the used catalysts were recorded during temperature-programmed desorption (TPD), when the catalysts were heated in the same manner as that for the TPO experiments but in a stream of nitrogen, without being exposed to oxygen. Apparently, all carbonaceous materials deposited on the Fe/TiO_2 catalyst were removed at 450°C just by the heat treatment. On the other hand, in the case of the Fe/Al_2O_3 catalyst, even after 30 min at 500°C the infrared spectrum showed two strong bands at 1569 and 1462 cm^{-1}. This amplifies the earlier assignment of these bands to polyaromatic species deposited on the Fe/Al_2O_3 catalyst and excludes the existence of such species on the Fe/TiO_2 catalyst. Considering the frequencies of the infrared bands below 1700

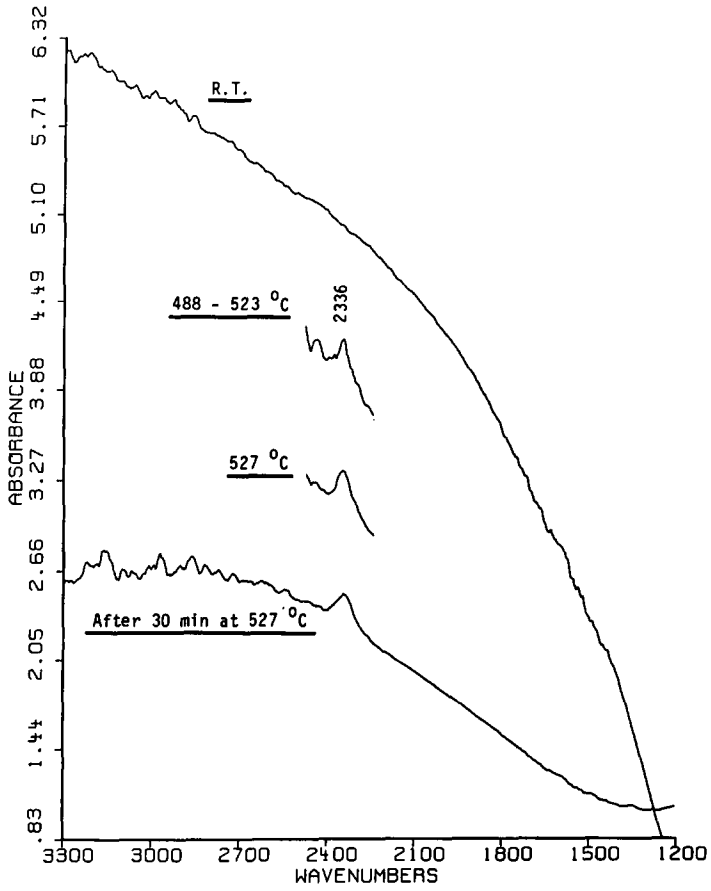

FIG. 5. Infrared spectra of Fe/ZrO_2 used catalyst. Spectra were recorded during TPO as indicated by arrows on curve (d) in Fig. 1.

cm^{-1} (*17,27*) for the used Fe/TiO_2 catalyst and the fact that a thermal treatment was sufficient to decompose and then desorb the materials associated with these bands, the presence of various forms of surface carbonates is postulated on the used Fe/TiO_2 catalyst. A contribution of surface carboxylates cannot be excluded.

Fe/ZrO_2 catalyst. An infrared spectrum of the used Fe/ZrO_2 catalyst recorded at room temperature before TPO is shown in Fig. 5. The catalyst was almost opaque to the infrared beam and had to be diluted with KBr at a weight ratio of 1 : 2 to allow recording of a spectrum. No infrared bands were observed in the spectral range 1200–3300 cm^{-1}. However, infrared spectra of the used catalyst without KBr diluent were recorded after the sample was oxidized above 450°C during TPO. The infrared band at 2336 cm^{-1}, which is characteristic of CO_2, was the only band observed. Apparently, an infrared inactive form of carbonaceous deposits, which produced CO_2 upon oxidation, existed on the used Fe/ZrO_2 catalyst.

Methylene groups. The calculated relative intensity ratios of the $-CH_3$ (~2970 cm^{-1}) and $-CH_2-$ (~2925 cm^{-1}) associated infrared bands are 0.24, 0.81, and 0.69 for the used Fe/SiO_2, Fe/Al_2O_3, and Fe/TiO_2 catalysts, respectively. A much greater rela-

tive strength of the $-CH_3$ associated infrared bands for the oligomeric species in the spectra of used Fe/Al_2O_3 and Fe/TiO_2 catalysts indicates that they are either considerably more branched or have shorter chains than those formed on the Fe/SiO_2 catalyst. According to the empirical formulas derived by Jones (*28*) for the solutions of *n*-paraffin hydrocarbons, the intensity of the 2970 cm^{-1} (CH_3) band is $(8n + 258)$ and that of the 2925 cm^{-1} (CH_2) band is $(77n - 18)$, where n is the number of methylene groups in the chain. The numbers of methylene groups in hydrocarbon chains of the oligomeric species adsorbed on the Fe/SiO_2, Fe/Al_2O_3, and Fe/TiO_2 catalysts calculated by this infrared method are 25, 5, and 6, respectively. It must be recognized that the accuracy of this calculation depends very much on the arbitrary assumptions that the oligomers formed on catalysts are linear and that the above equations derived for hydrocarbon solutions can be applied to adsorbed species (*21, 22*). However, even if the accuracy of the above calculation is doubtful, the conclusion that the oligomers formed on the Fe/SiO_2 catalyst are either much less branched or have longer chains than those formed on the other catalysts seems to be unquestionable. Of course, it is not possible to judge whether these carbonaceous materials play the role of intermediates in the Fischer–Tropsch synthesis, since insufficient information is available. However, it is worth mentioning that the selectivity toward branched alcohols observed on the Fe/Al_2O_3 and Fe/TiO_2 catalysts was high and the fraction of internal C_4 olefins was large (*16*).

Mössbauer Spectroscopy

The ^{57}Fe Mössbauer spectra of the investigated catalysts in fresh and used form are shown in Figs. 6 and 7, respectively. The spectra differ drastically for different support materials. The results of the analysis based on the least-squares fits of the spectra are collected in Tables 3 and 4. The following spectral parameters are given: IS is the isomer shift (in reference to metallic α-Fe), which represents the valent state of iron (*s*-electron density at iron nuclei); QS is the electric quadrupole splitting, which represents the quadrupole interaction of iron nuclei with the electric field gradient created both by *d*-electron shell of iron ions and by nearest ions in the lattice; H_{eff} is the mean effective hyperfine magnetic field at iron nuclei; and A is the percentage area under each spectral component. Usually it is assumed that the Mössbauer area ratios are equal to a relative amount of the associated species. This approximation is commonly used in the pertinent literature (*29–35*), although it is valid only when bond strength of iron species or dispersion of the phases in question are not very different. The estimates of the sizes of the iron oxide particles given below have been based on the calibration data reported by Kündig *et al.* (*36*) and by Mørup *et al.* (*37*). However, it must be noted that such estimates are not unambiguous: especially when the spectrum is not magnetically split, assignment to α-Fe_2O_3 and particle size determination on the basis of IS and QS alone can only be tentative.

Fresh catalysts. The spectra of fresh catalysts contain both ferromagnetic (sextuplet) and paramagnetic (doublet) components. The spectrum of Fe/SiO_2 exhibits a relaxation pattern consisting of a sextuplet of broad lines (40% of a total spectral area) and a poorly resolved central doublet (60% in area), which may be ascribed respectively to very small particles of α-Fe_2O_3 (~9 nm) and lepidocrocite γ-FeOOH. The presence of γ-FeOOH in this catalyst may indicate that the process of thermal dehydration was in this case either not complete or reversed by a long exposure to the atmospheric moisture. The spectrum of Fe/Al_2O_3 consists mostly of a central doublet representing small (<13 nm) particles of α-Fe_2O_3, with only about 15% of the iron in the form of larger crystallites. The spectrum of Fe/TiO_2 consists of a sextuplet characteristic of large (>13 nm) particles of α-Fe_2O_3, but in addition it shows a central doublet (36% in area)

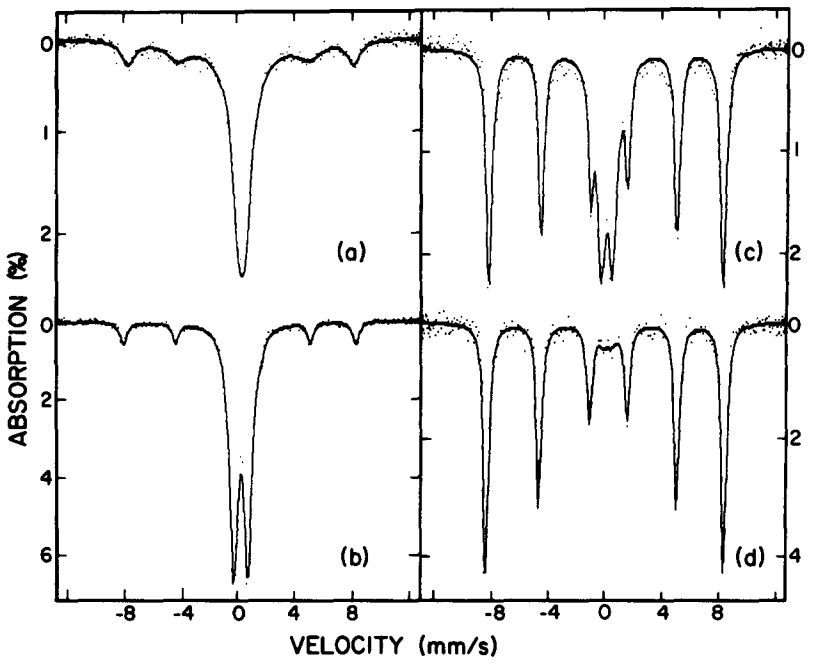

FIG. 6. ^{57}Fe Mössbauer spectra of fresh catalysts: (a) Fe/SiO_2, (b) Fe/Al_2O_3, (c) Fe/TiO_2, and (d) Fe/ZrO_2.

due to the presence of smaller particles. Finally, the spectrum of Fe/ZrO_2 shows a very well defined pattern of six narrow absorption lines, which indicates that all iron occurs in the form of well-defined particles of α-Fe_2O_3, with a diameter larger than 13 nm.

Small dimensions of iron oxide crystallites on the four support materials were confirmed by X-ray powder diffractograms.

TABLE 3

Computer-Fitted Parameters from Mössbauer Spectra of Fresh Catalysts Presented in Fig. 6

Catalyst	Component	IS (mm/s)	QS (mm/s)	H_{eff} (T)	A (%)
Fe/SiO_2	α-Fe_2O_3(~9 nm)	0.32	−0.13	48.6	40
	γ-FeOOH	0.39	0.49	—	60
Fe/Al_2O_3	α-Fe_2O_3(<13 nm)	0.38	−0.24	50.3	15
		0.33	0.99	—	85
Fe/TiO_2	α-Fe_2O_3(~13 nm)	0.37	−0.22	50.4	64
		0.34	0.78	—	36
Fe/ZrO_2	α-Fe_2O_3(>13 nm)	0.37	−0.20	51.2	100

TABLE 4

Computer-Fitted Parameters from Mössbauer Spectra of Used Catalysts[a] Presented in Fig. 7

Catalyst	Component	IS (mm/s)	QS (mm/s)	H_{eff} (T)	A (%)
Fe/SiO_2		0.25	0.04	22.5	
	χ-Fe_5C_2	0.23	0.04	17.6	53
		0.40	0.04	11.0	
	Fe_3O_4(6 nm)	0.63	−0.11	42.6	14
	Fe^{3+}	0.37	1.07	—	33
Fe/Al_2O_3		0.27	0.14	21.4	
	χ-Fe_5C_2	0.21	0.10	18.2	20
		0.36	0.04	11.3	
	Fe_3O_4(7 nm)	0.54	−0.10	44.6	6
	Fe^{3+}	0.38	1.00	—	55
	Fe^{2+}	0.97	2.14	—	19
Fe/TiO_2		0.19	0.11	21.0	
	χ-Fe_5C_2	0.18	0.00	18.7	10
		0.36	0.04	10.8	
	Fe^{3+}	0.36	0.71	—	52
	Fe^{2+}	1.08	0.77	—	38
Fe/ZrO_2		0.25	0.11	21.6	
	χ-Fe_5C_2	0.17	0.07	18.9	86
		0.22	0.11	11.1	
	Fe^{3+}	0.37	1.00	—	14

[a] Catalysts exposed to air before measurements.

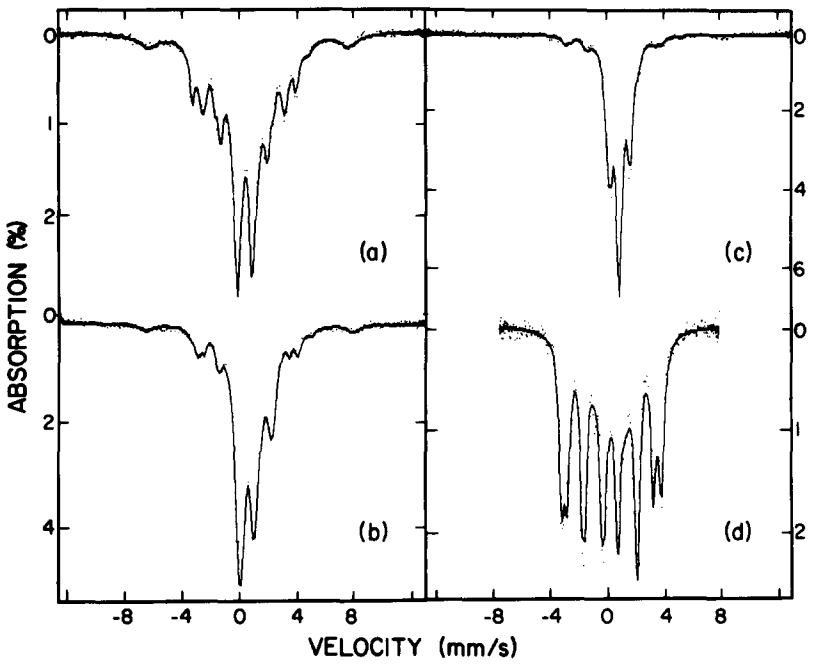

FIG. 7. ^{57}Fe Mössbauer spectra of used catalysts: (a) Fe/SiO_2, (b) Fe/Al_2O_3, (c) Fe/TiO_2, and (d) Fe/ZrO_2.

Well-defined narrow peaks of Fe_2O_3 could only be distinguished on the diffractograms of Fe/ZrO_2 and Fe/TiO_2, whereas only very broad poorly defined peaks due to iron oxide crystallites could be seen in the case of Fe/Al_2O_3 and Fe/SiO_2. The sizes of iron oxide crystallites, as estimated from the broadening of the diffraction lines using the Scherrer formula, were in fairly good agreement with those determined from the Mössbauer spectra.

From these results it can be inferred that in the fresh catalysts the order of increasing the average size of iron oxide particles was Fe/SiO_2, Fe/Al_2O_3, Fe/TiO_2, and Fe/ZrO_2. Thus, the observed size of iron oxide particles is clearly correlated with the surface area of the oxides used as the support materials.

Used catalysts. Mössbauer spectra of the catalysts used in the Fischer–Tropsch synthesis for 260 h are shown in Fig. 7. Generally, the spectra represent the superposition of iron carbides and iron oxide patterns. The spectrum of the Fe/ZrO_2 catalyst has been best fitted with three carbide sextets, with the hyperfine fields H_{eff} = 22, 19, and 11 T. Consistent with the literature data (*33–35*), such a spectrum can be attributed to Hägg carbide, χ-Fe_5C_2. The spectrum of used Fe/SiO_2 indicates the 53% fraction of χ-Fe_5C_2 carbide in addition to very finely divided Fe_3O_4 particles (14%) and Fe^{3+} species (33%). In Fe/Al_2O_3 and Fe/TiO_2, the fraction of χ-Fe_5C_2 was only ~20 and ~10%, respectively. In the spectrum of the Fe/TiO_2 catalyst, the remaining peaks could be attributed to Fe^{3+} species and Fe^{2+} species. A significant fraction of the Fe^{2+} species (~20%) has been also observed in the used Fe/Al_2O_3 catalyst.

In the X-ray diffractograms the presence of the carbide crystallites was clearly indicated only in the case of the Fe/ZrO_2 catalyst. In other catalysts the carbide particles were either too small or too poorly crystallized to exhibit any diffraction features.

Since all used catalysts were exposed to

air at room temperature it is likely that iron species that might exist in the working catalysts were converted to iron oxides. Whether air exposure at room temperature oxidizes carbonaceous deposits or not is debatable. Although direct experimental evidence that would fully exclude such a possibility is not available, it does not seem highly plausible. TPO experiments showed that temperatures higher than 100°C were required to commence weight loss due to carbonaceous materials oxidation. Also, oxygenated carbonaceous materials were detected by FTIR only on the Fe/Al_2O_3 and Fe/TiO_2 catalysts for reasons other than air exposure, as discussed later.

Reoxidized catalysts. Specimens of spent catalysts were heated in air at 400°C for 10 min. The Mössbauer spectra (not shown) measured after heating revealed in each case Fe^{3+} in a form of α-Fe_2O_3 particles with a dispersion similar to that observed in fresh catalysts. This proves that the carbides decompose fairly easily and oxidize upon heating in the presence of oxygen. This result agrees with the FTIR and TPO data obtained at similar conditions for the same specimens.

CONCLUSIONS

Any species containing carbon formed on a catalyst surface during Fischer–Tropsch synthesis was classified in this work as a carbonaceous material. This definition goes beyond the narrower and somewhat arbitrary description of carbonaceous materials presented in the literature [e.g. (*9, 10*)]. The forms of carbonaceous deposits identified in this work are summarized in Table 5.

It is obvious that characteristics of the carbonaceous materials were strongly influenced by the nature of the support. In the present study direct experimental evidence has been obtained for the existence of all forms of deposits except for amorphous carbon postulated to be present on Fe/SiO_2. The latter was infrared inactive, could not be removed from the catalyst surface by simple heat treatment, and did not contribute to the Mössbauer spectra of carbides. A temperature of 550°C was necessary to oxidize this carbonaceous material. Therefore, the assignment of the amorphous form of carbon is, although logical, somewhat speculative as direct experimental evidence is not presently available. It should be noted, however, that amorphous carbon does not have an obvious characteristic feature that is easy to determine experimentally. Since all catalysts were removed from the reactor in their active state after steady-state conditions were reached, it is very likely that at least part of the carbonaceous materials accumulated on the catalyst surface, besides well documented carbides, played some role as an active intermediate in the synthesis.

The most challenging assignment would be to elucidate correlation between significant factors related to the nature of a catalyst support and the characteristics of carbonaceous materials. A complete picture cannot be given as too many variables must be considered. However, a tentative relationship based on this study is offered.

The formation of oxygenated forms of carbonaceous deposits on Fischer–Tropsch catalysts, such as carbonates and carboxylates, is not very well documented in the literature. Their influence on the catalytic performance of these catalysts is not known. It is very likely that these forms of carbonaceous materials on the Fe/Al_2O_3 catalyst are linked with the ability of alumina support (*17, 23*) to contribute lattice oxygen for oxidized moiety. The abundance of similar moieties on the used Fe/TiO_2 catalyst may be explained by the presence of titania species (TiO_x) (*38*) on the surface of metal particles during Fischer–Tropsch synthesis. It has been suggested (*38*) that the TiO_x species resulted from the reducibility of titania support and the strong metal support interaction and that they might maintain an appropriate amount of oxygen on the surface, which in turn might control the balance between "active" and "inactive" carbon species. In the present study

TABLE 5

Forms of Carbonaceous Deposits on Supported Iron Catalysts Observed or Elucidated from the Present Study

Catalyst	Form of carbonaceous deposit				
	Aliphatic	Aromatic	Oxygenated	Carbidic	Amorphous
Fe/SiO_2	○			○	○
Fe/Al_2O_3	○	○	○	○	
Fe/TiO_2	○		○	○	
Fe/ZrO_2				○	

only a small fraction of Fe (~10%) has been seen in carbides on the used Fe/TiO_2 catalyst, but substantial amounts of the carbonaceous oxidized moieties were detected. One may speculate that the rate-determining step is shifted to CO dissociation on Fe/TiO_2 and the fast hydrogenation of "active" carbon (*39*) does not allow the iron carbide buildup. Oxygen of the titania support may be used to convert either CO or surface carbon into inactive oxidized moieties.

In the present study, undoubtedly, the particle size of iron oxide in fresh catalysts seemed to be correlated with surface area. It is likely that after reduction such a correlation will hold. Nevertheless, particles of iron oxides in the fresh Fe/ZrO_2 catalyst were the largest as confirmed by Mössbauer spectroscopy. The influence of metal particle size on the morphology of carbonaceous deposits seems to be well documented, at least in the case of filamentous carbon formation, which involves carbide participation (*40, 41*). It is postulated here that the almost complete conversion of iron into iron carbides detected in the used Fe/ZrO_2 catalyst is related to the large particles of iron (oxide).

High acidity of the alumina support may stimulate the aromatic character of the carbonaceous deposit (*42, 43*). A significant portion of the carbonaceous materials may be deposited on the support itself (*17, 44*). Convincing experimental evidence of direct attachment to iron was presented only for carbides. On the other hand, basicity of the SiO_2 support may be responsible for long carbon chain oligomers (*45*) detected on the used Fe/SiO_2 catalyst, as discussed previously. Also, it has been noted that the rate of carbon hydrogenation is relatively low on silica-supported catalysts (*39*) because of support basicity (*45*). This may explain the accumulation of the amorphous carbons detected on the used Fe/SiO_2 catalyst in the present study. Further studies are required to derive better correlations.

Resistance to reduction of the supported iron catalysts has been noted in a rather small part of the relevant literature, which dealt mainly with Mössbauer investigations. It has been explained by strong support metal interaction [TiO_2 (*38*), Al_2O_3 (*35*)], surface decoration [SiO_2 (*46*)], or formation of chemical compounds on the surface of the catalysts [Al_2O_3 (*35, 38, 47*), SiO_2 (*31, 48*)]. It has been stated (*31*) that the reduction behavior of supported iron catalysts is not well understood since it depends on iron loading, the preparation method, and pretreatment conditions. However, it is likely that significant amounts of iron oxides coexist with the metallic iron and the iron carbides even at Fischer–Tropsch synthesis conditions. These oxides may also contribute oxygen for the formation of carbonates and carboxylate species detected in the present study of alumina- and titania-supported iron catalysts. Also, unreduced iron oxide phases can catalyze a water–gas-shift (WGS) reaction (*49*), which may result in promotion of lighter hydrocarbon formation.

ACKNOWLEDGMENTS

The authors thank Dr. T. Wrzesniewska for the SEM analysis and Mr. R. Dureau for the technical assistance with the TGA experiments.

REFERENCES

1. Rabo, J. A., Risch, A. P., and Poutsma, M. L., *J. Catal.* **53,** 295 (1978).
2. McCarty, J. G., and Wise, H., *J. Catal.* **57,** 406 (1979).
3. Biloen, P., Helle, J. N., and Sachtler, W. M. H., *J. Catal.* **58,** 95 (1979).
4. Bonzel, H. P., and Krebs, H. J., *Surf. Sci.* **91,** 499 (1980).
5. Ott, G. L., Fleisch, T., and Delgass,W. N., *J. Catal.* **65,** 253 (1980).
6. Bonzel, H. P., and Krebs, H. J., *Surf. Sci.* **109,** L527 (1981).
7. Galuszka, J., Chang, J. R., and Amenomiya, Y., *J. Catal.* **68,** 172 (1981).
8. Kieffer, E., and van der Baan, H. S., *Appl. Catal.* **3,** 245 (1982).
9. Bartholomew, C. H., *Catal. Rev.-Sci. Eng.* **24,** 67 (1982).
10. Wolf, E. E., and Alfani, F., *Catal. Rev.-Sci. Eng.* **24,** 329 (1982).
11. Reymond, J. P., Meriaudeau, P., and Teichner, S. J., *J. Catal.* **75,** 39 (1982).
12. Komiya, M., Tsunoda, T., and Ogino, Y., *Carbon* **23,** 613 (1985).
13. Choi, J.-G., Rhee, H.-K., and Moon, S. H., *Appl. Catal.* **13,** 269 (1985).
14. Bartholomew, C. H., Strasburg, M. V., and Hsien, H.-Y., *Appl. Catal.* **36,** 147 (1988).
15. Bianchi, D., and Gass, J. L., *J. Catal.* **123,** 298 and 310 (1990).
16. Sano, T., and Galuszka, J., to be published.
17. Galuszka, J., and Amenomiya, Y., in "Proceedings, 9th International Congress on Catalysis, Calgary 1988" (M. J. Phillips and M. Ternan, Ed.), Vol. 2, p. 697. Chem. Institute of Canada, Ottawa, 1988.
18. Sawicki, J. A., Rolston, J. H., Julian, S. R., Tyliszczak T., and McCrimmon, K. D., *Mater. Res. Soc. Symp. Proc.* **111,** 65 (1986).
19. Sheppard, N., and Ward, J. W., *J. Catal.* **15,** 50 (1969).
20. Greenler, R. G., *J. Chem. Phys.* **37,** 2094 (1962).
21. Eisenbach, D., and Gallei, E., *J. Catal.* **56,** 377 (1979).
22. Ghosh, A. K., and Kydd, R. A., *J. Catal.* **100,** 185 (1986).
23. Najbar, J., and Eischens, R. P., *in* "Proceedings, 9th International Congress on Catalysis, Calgary 1988, (M. J. Phillips and M. Ternan, Ed.), Vol. 3, p. 1434. Chem. Institute of Canada, Ottawa, 1988.
24. Lox, E. S., Marin, G. B., Grave, E., and Bussiere, P., *Appl. Catal.* **40,** 197 (1988).
25. Fukushima, T., Arakawa, H., and Ichikawa, M., *J. Chem. Soc. Chem. Commun.*, 729 (1985).
26. Underwood, R. P., and Bell, A. T., *J. Catal.* **111,** 325 (1988).
27. Little, L. H., "Infrared Spectra of Adsorbed Species," pp. 74–83. Academic Press, London/New York, 1966.
28. Jones, R. N., *Spectrochim. Acta* **9,** 235 (1957).
29. Niemantsverdriet, J. W., van der Kraan, A. M., van Dijk, W. L., and van der Baan, H. S., *J. Phys. Chem.* **84,** 3365 (1980).
30. Niemantsverdriet, J. W., van der Baan, A. M., Delgass, W. N., and Vannice, M. A., *J. Phys. Chem.* **89,** 67 (1985).
31. van der Kraan, A. M., *Hyperfine Interact.* **40,** 211 (1988).
32. van der Kraan, A. M., and Niemantsverdriet, J. W., *in* "Industrial Applications of the Mössbauer Effect" (G. J. Long and J. G. Stevens, Eds.), p. 609. Plenum, New York. 1986.
33. Caër, G. L., Dubois, J. M., and Senateur, J. P., *J. Solid State Chem.* **19,** 19 (1976).
34. Caër, G. L., Dubois, J. M., Pijolat, M., Perrichon, V., and Bussière, P., *J. Phys. Chem.* **86,** 4799 (1982).
35. Lee, J.-F., Lee, M.-D., and Tseng, P.-K., *Appl. Catal.* **52,** 193.(1989).
36. Kündig, W., Bömmel, H., Constabaris, G., and Lindquist, R. H., *Phys. Rev.* **142,** 933 (1966).
37. Mørup, S., and Topsøe, H., *Appl. Phys.* **11,** 63 (1976).
38. Jiang, X-Z., Stevenson, A., and Dumesic, J.A., *J. Catal.* **91,** 11 (1985).
39. Bartholomew, C. H., and Vance C.K., *J. Catal.* **91,** 78 (1985).
40. Galuszka, J., and Back, M. H., *Carbon* **22,** 141 (1984).
41. Baker, R. T. K., and Harris, P. S., "Chemistry and Physics of Carbon" (P. L. Walker, Jr., and P. A. Thrower, Eds.), Vol. 14, p. 83. Dekker, New York, 1978.
42. Csicsery, M. S., *Ind. Eng. Chem. Process Des. Dev.* **18,** 2 (1979).
43. Bragin, O. V., *Russ. Chem. Rev.* **50,** 1045 (1981).
44. Gallezot, P., Leclercq, C., Barbier, J., and Marecot, P., *J. Catal.* **116,** 164 (1989).
45. Snel, R., *Catal. Rev.-Sci. Eng.* **29,** 361 (1987).
46. Lund, C. R. F., and Dumesic, J. A., *J. Catal.* **72,** 21 (1981).
47. Vaishnava, P. P., Ktorides, P. I., Montano, P. A., Mbadcam, K. J., and Melson, G. A., *J. Catal.* **96,** 301 (1985).
48. Wielers, A. F. H., Kock, A. J. H. M., Hop, C. E. C. A., Geus, J. W., and van der Kraan, A. M., *J. Catal.* **117,** 1 (1989).
49. Reuel, R. C., and Bartholomew, C. H., *J. Catal.* **85,** 78 (1984).